Decolorization effect and related mechanism of atmospheric pressure plasma jet on Eriochrome Black T

Xiaoyan Li, Jinren Liu, Yueming Wu, Lingge Gao, Yan Ma, Guimin Xu, Guoqiang Li, Longlong Zhang, Miao Li, Li You, Xingmin Shi and Wang Yuan

ABSTRACT

In this study, Eriochrome Black T (EBT) in water was decolorized by means of argon atmospheric pressure plasma jet (APPJ), which showed great decolorization performance. The results showed that the relatively high decolorization rate (approximately 80%) was obtained after plasma treatment for 6 min. Changes to some reactive oxygen and nitrogen species (RONS) in the liquid phase were detected. The contents of peroxide, HO·, O_2^-·, and NO· in the plasma-treated EBT solution were much less than those in the activated water. The roles of H_2O_2 and HO· in the decolorization of EBT solution were explored by evaluating the effects of their scavengers, and by exploring the direct effect of H_2O_2. The results indicated that reactive oxygen species (ROS), especially HO· and O_2^-·, played significant roles in the decolorization of the EBT solution. Analysis of degradation by-products indicated that plasma discharge could destroy the azo bond first and gradually break the aromatic rings of EBT molecules into small molecular compounds.

Key words | atmospheric pressure plasma jet (APPJ), decolorization, Eriochrome Black T (EBT), reactive oxygen and nitrogen species (RONS)

Xiaoyan Li
Jinren Liu
Yueming Wu
Lingge Gao
Yan Ma
Xingmin Shi (corresponding author)
School of Public Health, Medical Science Center,
Xi'an Jiaotong University,
Xi'an 710061, China
E-mail: *shixingmin142@163.com*

Xiaoyan Li
Miao Li
School of Nursing,
Xi'an Siyuan University,
Xi'an 710038, China

Guimin Xu
Guoqiang Li
State Key Laboratory of Electrical Insulation and Power Equipment, School of Electrical Engineering,
Xi'an Jiaotong University,
Xi'an 710049, China

Longlong Zhang
Li You
School of Education,
Xi'an Siyuan University,
Xi'an 710038, China

Wang Yuan
Department of Diagnostic Radiology, the First Hospital of Medical Science Centre,
Xi'an Jiaotong University,
Xi'an 710061, China

INTRODUCTION

Dyes make our world colorful. However, during the production and utilization of dyes, a large amount of dye wastewater is discharged into the environment, which is highly chromatic, toxic, complex and non-biodegradable. Dyes discharged in water could disrupt the ecosystem, affecting the photosynthesis in water plants (Crini 2006). Therefore, the removal of color from dye wastewater is a primary issue.

Azo dyes are widely used in the printing and dyeing industries, which account for almost half of all dyes. A number of synthetic azo dyes have been suspected to be carcinogenic, teratogenic and mutagenic (Rawat *et al.* 2018). The molecular structure of azo dyes contains one or more azo bonds (–N = N–) and aromatic structures, which make the dyes hard to degrade. During the natural degradation process, azo bonds can be reduced to aromatic amines, and the 'triple effects' of aromatic amines become even stronger.

Traditional chemical, physical and biological processes to treat wastewater containing textile dyes have such

doi: 10.2166/wst.2019.120

disadvantages as high cost, high energy requirement and generation of secondary pollution (Kalsoom *et al.* 2015). Moreover, these traditional wastewater treatment techniques are usually ineffective for the degradation of refractory organics.

Recently, advanced oxidation techniques and processes (AOPs), characterized by the production of hydroxyl radicals (HO·) with strong oxidizing power, have been gradually applied in the treatment of refractory organics (Kabdasli *et al.* 2015). AOPs have been proven to be powerful and efficient for degrading recalcitrant materials and toxic contaminates (Vilar *et al.* 2017). Low temperature plasma (LTP), usually generated at room temperature under atmospheric pressure, has been claimed to be rich in charged particles, various free radicals and other active ingredients (Setsuhara 2016; Chauvin *et al.* 2017). Various kinds of LTPs have been employed for water treatment to reduce organic pollutants such as dyes (Olszewski *et al.* 2014; Garcia *et al.* 2017), phenolic compounds (Krugly *et al.* 2015), and antibiotics (Tran *et al.* 2017).

Atmospheric pressure plasma jet (APPJ) is an emerging LTP generation technique. APPJ is operated at atmospheric pressure, with the advantages of an open system, spatial separation and easy operation (Garcia *et al.* 2017). It has shown good application prospects in many fields, such as biomedicine, material processing, and environmental protection. The gas plasma produces reactive species including charged particles, excited particles, ultraviolet photons, radicals, and other ground state particles. APPJ carries and spreads them on the liquid surface so that reactions can take place at the gas and aqueous solution interface. The reactive oxygen and nitrogen species (RONS), including HO·, hydrogen peroxide (H_2O_2), ozone (O_3), superoxide anion (O_2^-·), nitric oxide (NO·) and peroxynitrite anion ($ONOO^-$) are generated in aqueous solution. RONS will play very important roles in the decolorization process.

Eriochrome Black T (EBT), a typical azo dye, was selected as a model pollutant in our experiment. The chemical structure of EBT (Abdelmalek *et al.* 2006) contains an azo bond and two naphthalene rings. At present, there are a few reports on the degradation of EBT by LTP; however, the degradation mechanism remains unclear as yet (Zaghbani *et al.* 2009; Djomgoue *et al.* 2015; Karimi *et al.* 2018). In this study, the decolorization effect of APPJ on the model wastewater of EBT was investigated for the first time, especially the roles of RONS in decolorization. The related mechanism and possible degradation pathways of EBT by APPJ were also discussed.

MATERIAL AND METHODS

In this study, all reagents used were of analytical grade. And all solutions were prepared using de-ionized water.

Model wastewater

The EBT was purchased from No.3 Branch of Shanghai Reagent Plant. The molecular formula of EBT is $C_{20}H_{12}O_7N_3SNa$, and the molecular mass is 461.39. A stock solution (1,000 mg·L^{-1}) was prepared by dissolving EBT in de-ionized water, which was protected from light at low temperature. The stock solution was diluted on site to obtain experimental model wastewater of 50 mg·L^{-1} EBT.

Experimental setup

The experimental setup is shown in Figure 1(a) and 1(b). A hollow quartz tube is used as the barrier dielectric, which has inner and outer diameters of 2.0 and 4.0 mm, respectively. Two copper strip electrodes with 10.0 mm width are wrapped around the tube. The electrode near the nozzle is grounded, the other one is connected to high voltage. The grounded electrode is 10.0 mm from the nozzle and 16.5 mm from the power electrode. The high voltage is applied between the two electrodes to ignite the discharge. The peak-to-peak value of the applied voltage was about 15.0 kV. The frequency was 39.5 kHz and the discharge power was about 10 W. The working gas was argon with a flow rate of 0.5 slm. A cold atmospheric pressure plasma jet was formed by the flowing argon gas. The temperature at the tip of the APPJ varied from 25 to 36 °C, which was measured by an alcohol thermometer. Figure 1(c) shows the waveform of the applied voltage and circuit current. A high-voltage TekP6015A probe measured the voltage waveform (1000:1). The current waveform was obtained by measuring the voltage across a non-inductive resistor R_m (50Ω) in series. The emission spectrum of the plasma jet was measured with a spectrometer (Mechelle 5000, Andor Technology Ltd, Belfast, UK) and an enhanced charge-coupled device (ICCD) (iStar334, Andor Technology Ltd, Belfast, UK).

Plasma treatment

When the device could stably produce plasma, 1 mL EBT solution (50 mg·L^{-1}) was added into a 24-well plate (Corning, USA) and placed vertically under the APPJ generating

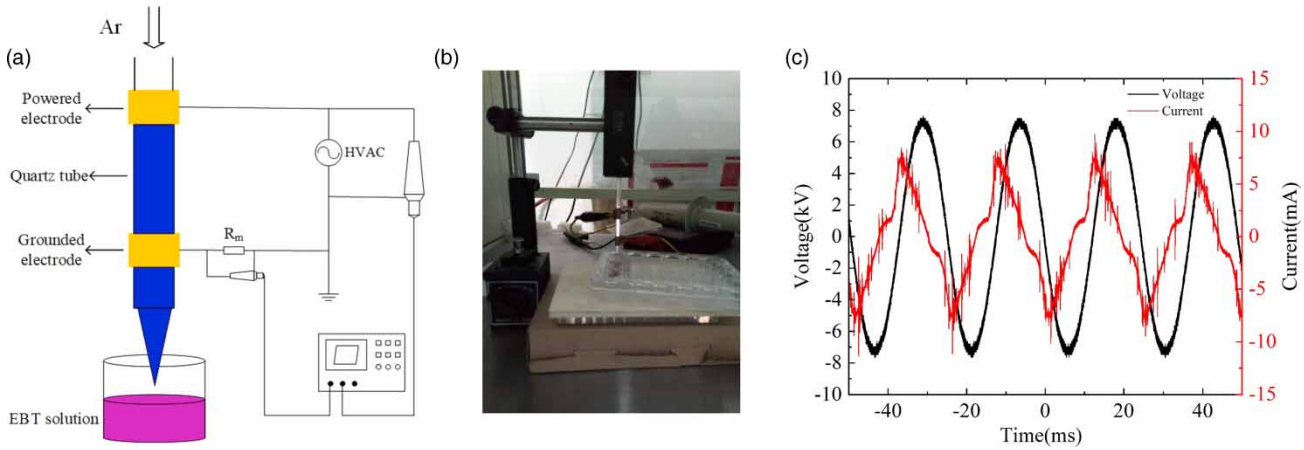

Figure 1 | Diagram (a) and picture (b) of the APPJ generating experimental setup, voltage and current waveform (c) applied.

setup. The distance from the liquid surface to the quartz tube lower port was 1.0 cm. The tip of the plasma was close to the surface but did not contact it. The treatment times were 0, 2, 4, 6, 8, and 10 min.

Decolorization effect

According to the Beer-Lambert Law, the absorbance is proportional to the concentration of EBT molecules in solution. Therefore, the decolorization rate can reflect the degradation of EBT in solution. During our experiment, an 0.2 mL EBT sample was added to a 96-well plate (Corning, USA) and the absorbance at 525 nm (A_{525}) was recorded on an Infinite M200 microplate reader (Tecan, Switzerland). The decolorization effect of APPJ on EBT solution was evaluated by the decolorization rate (η), and calculated according to formula (1):

$$\eta = \frac{A_0 - A_t}{A_0} \times 100\% \quad (1)$$

where A_0 and A_t stand for the absorbance at 525 nm of EBT solution with plasma exposure for 0 and t min, respectively.

Determination of RONS in EBT solution and activated water

To explore the related mechanism of APPJ on EBT solution, we determined the changes of peroxide (including H_2O_2 and $ONOO^-$), $HO\cdot$, $O_2^-\cdot$, and $NO\cdot$ in the activated water and EBT solution after plasma treatment. The de-ionized water was treated by APPJ in the same way as the EBT solution was treated to obtain activated water. The treatment times were 0, 1, 2, 3, 4, 5 and 6 min.

In this study, the peroxide concentration in solution was determined by coumarin boronic acid (CBA) probe (Liu *et al.* 2017). Firstly, 2 μl CBA was added into 1 mL activated water or plasma-treated EBT solution, incubated for 15 min at 40 °C. Secondly, the fluorescence intensity of COH was detected with a microplate reader at the excitation wavelength (355 nm) and emission wavelength (460 nm). Thirdly, the concentration of peroxide was quantified based on the H_2O_2 standard curve. The production capacities of $HO\cdot$ and $O_2^-\cdot$ in solution were determined with a hydroxyl radical assay kit and a superoxide anion generation kit (Jiancheng Bioengineering Institute, Nanjing, China), respectively (Liu *et al.* 2017; Shi *et al.* 2018). The $NO\cdot$ produced by plasma quickly converted to nitrate (NO_3^-) and nitrite (NO_2^-). Therefore, the total amount of NO_3^- and NO_2^- was determined with a nitric oxide kit (Biyuntian Biotechnology Co., Ltd, Shanghai, China), to represent the total content of RNS (Shi *et al.* 2015).

The measurement principles of $O_2^-\cdot$ are listed as follows. The reaction system simulates the reaction of xanthine and xanthine oxidase to produce $O_2^-\cdot$, which can oxidize hydroxylamines to form NO_2^-. When the electron acceptors are provided, NO_2^- reacts with Griess reagent and forms violet compounds. The color depth of the solution is proportional to $O_2^-\cdot$ in a certain range. The operation procedures were performed according to the manufacturer's specification. The absorbance at 550 nm was measured with a microplate reader.

The 1 U/L $O_2^-\cdot$ in solution is defined to be equivalent to 1 mg of ascorbic acid by consuming $O_2^-\cdot$ in the reaction system under the reaction conditions. The effect of the sample on $O_2^-\cdot$ could be determined to compare it with the standard material (ascorbic acid), according to

formula (2):

$$O_2^-\cdot\text{production (U/L)} = \frac{A_T - A_C}{A_C - A_S} \times C_S \times 1000\ \text{mL} \times k \qquad (2)$$

where A_T, A_C, A_S stands for the absorbance at 550 nm of the test (solution treated by APPJ), control (distilled water) and standard (ascorbic acid) tubes, respectively; k is the dilution ratio of the sample before the test, which was 1 in our experiments; C_S denotes the concentration of standard, equal to 0.15 mg·mL^{-1}. The positive value indicates that the sample contains the substance producing $O_2^-\cdot$, while the negative value indicates that the sample contains a substance that could consume $O_2^-\cdot$.

In order to verify the roles of H_2O_2 and HO· in the decolorization of dye molecules, the effects of their scavengers were explored. As catalase (CAT) and ascorbic acid are the scavengers for H_2O_2 and HO·, respectively, the EBT solution with 2 ‰ (V: V) CAT and 40 μM ascorbic acid were treated by the plasma. The H_2O_2 reagent, whose concentration was equal to peroxide (standardized by H_2O_2) in each group of the activated water, was added into the EBT solution. The absorbance of the EBT solution was measured with a microplate reader after 10 min.

Evaluation of degradation residues

The UV/VIS spectra of plasma-treated EBT solutions were obtained by a microplate reader in a range from 250 to 800 nm. Fourier-transform infrared spectroscopy (FTIR) was applied to identify the characterization of the chemical bonds of the EBT before and after plasma treatment. For each sample, 15 mL was collected, dried at 80 °C in a water bath, and then dried at 105 °C for 30 min. The solid samples were mixed with KBr solid powder homogenously in an agate mortar and then compressed to disks, scanned in a range from 4,000 to 500 cm^{-1} using an FTIR spectrometer (AVATAR 330FT-IR Thermo Nicolet); 100 scans were taken at a resolution of 4 cm^{-1}.

Statistical analysis

Each experiment was repeated three times. All data were processed with SPSS (Version XIII) and analyzed with one-way analysis of variance (ANOVA). The experimental results were shown as mean ± standard deviation. $P < 0.05$ was considered statistically significant.

RESULTS AND DISCUSSION

The emission spectra of APPJ

The emission spectrum of APPJ recorded in the wavelength range of 300 to 900 nm is shown in Figure 2. We found that most of the lines were metastable argon atoms. The emission lines of HO· (309 nm), NO· (334.8 nm), N_2 (380.4 nm), and the excited O atom (673.0 nm) were also presented. The excited O atoms and HO· are highly active free radicals that have a destructive effect on the refractory organics (Karthikeyan *et al.* 2015), can react with the dye molecules at the gas-liquid interface and degrade them.

The water molecules in the solution evaporate into the ambient air to form humid air, and change the chemical properties of the plasma in the gas phase. Before reaching the liquid, the flowing argon gas blows out the plasma generated in the discharge region and contacts with humid air. Energetic metastable argon atoms (Ar^m) are able to cause excitation of nitrogen and oxygen molecules, thus producing reactive species containing nitrogen or oxygen (such as N_2, NO·, O, HO·, etc.). The previous study (Garcia *et al.* 2017) suggested that argon species were very important in the transformation of these species. Related reactions were described as the following reactions (Olszewski *et al.* 2014; Shi *et al.* 2018).

$$N_2 + Ar^m \rightarrow N_2\cdot + Ar \qquad (3)$$

$$N_2\cdot + H_2O_{(gas)} \rightarrow HO\cdot + H + N_2 \qquad (4)$$

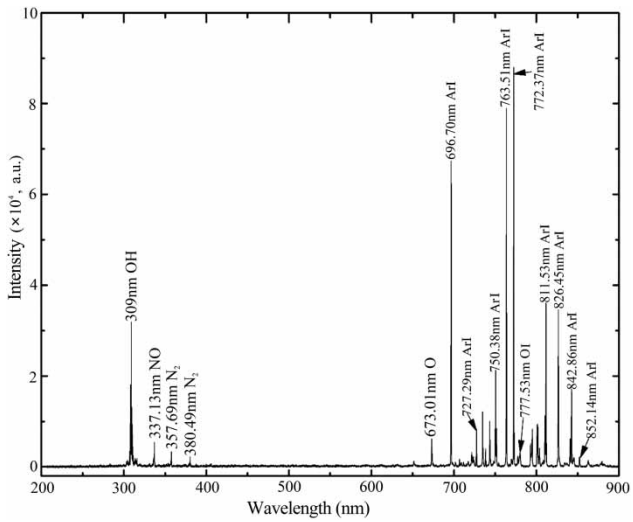

Figure 2 | Emission spectrum of APPJ.

$$H_2O_{(gas)} + Ar\cdot \rightarrow HO\cdot + H + Ar \quad (5)$$

$$O + H_2O \rightarrow HO\cdot + HO\cdot \quad (6)$$

$$H_2O_2 + HO\cdot \rightarrow H_2O + HO_2\cdot \quad (7)$$

$$H_2O + O_3 \rightarrow 2HO\cdot \quad (8)$$

$$N_2 + O \rightarrow NO + N \quad (9)$$

$$O + O_2 \rightarrow O_3 \quad (10)$$

$$NO + O_3 \rightarrow NO_2 + O_2 \quad (11)$$

Decolorization effect of APPJ

The feasibility of EBT degradation by APPJ was investigated. Obviously, great decolorization performance was observed. As a result, the color of the EBT solution gradually became lighter from the initial purple color with extension of the treatment time (Figure 3(a)). The color change of the EBT solution was observed as a result of the major reaction intermediates, which could be an indicator of the level of degradation. The results indicated that the EBT concentration steadily decreased.

The decolorization rate of plasma-treated EBT solution is shown in Figure 3(b). As can be seen, the decolorization rate increased gradually with prolongation of APPJ treatment time. It could reach approximately 80% after 6 min of plasma treatment, indicating that APPJ could destroy the EBT dye molecules rapidly and effectively. However, there were no significant differences among the treatments of 6, 8 and 10 min ($P > 0.05$). Therefore, the longest treatment time was set to be 6 min in the hereafter reported experiments. In the process of plasma treatment, the reactive species gradually increased and reacted with dye molecules in solution. The chromogenic groups in EBT molecules were destroyed and the EBT solution faded.

The change of pH value is related to the solute in the solution. The effect of APPJ treatment on the pH of the EBT solution is presented in Figure 3(c). During the treatment process, the pH of the EBT solution dropped rapidly from 4.69 ± 0.19 to 2.93 ± 0.12, especially during the early stage of treatment. In the experiment, we found that the pH change of the EBT solution was consistent with that of A_{525}. Tentative inferences on this result are as follows: on one hand, it was related to the presence of nitrite and nitrate ions in the solution; on the other hand, a large number of acidic substances such as organic acids were probably produced during the plasma treatment process.

Evolution of RONS in EBT solution and activated water

The reactive species generated by the plasma are transported into the aqueous solution and complex chemical reactions take place with water molecules, organic solutes, and inorganic solutes (such as O_2 and N_2) at the gas-liquid interface. The reactive species generated in aqueous solution mainly include reactive oxygen species (ROS), such as $O_2^-\cdot$, $HO\cdot$, O_3^-, and H_2O_2, and reactive nitrogen species (RNS),

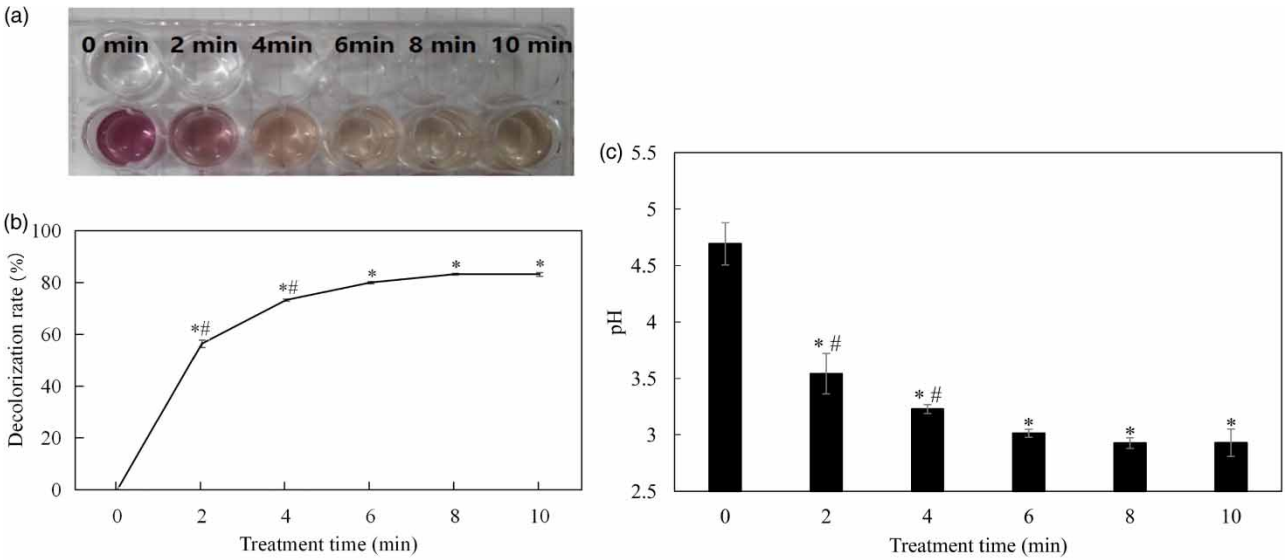

Figure 3 | The effect of APPJ on EBT solution with different treatment times, color change (a), decolorization rate (b), pH change (c). The error bars showed the standard deviation of replications. * $P < 0.05$ versus the original EBT solution, # $P < 0.05$ versus EBT solution treated by plasma for 6 min.

such as NO·, NO_2, and $ONOO^-$, in accordance with the following reactions (Jiang *et al.* 2012; Chen *et al.* 2017; Garcia *et al.* 2017):

$$O_2 + e \rightarrow O + O + e \quad (12)$$

$$O_2 + O \rightarrow O_3 \quad (13)$$

$$O_2 + e \rightarrow O_2^-\cdot \quad (14)$$

$$O_2^-\cdot + H^+ \rightarrow HO_2^- \quad (15)$$

$$O_2^-\cdot + HO_2\cdot \rightarrow HO_2^- + O_2 \quad (16)$$

$$HO_2^- + H_2O \rightarrow H_2O_2 + OH^- \quad (17)$$

$$2HO_2\cdot \rightarrow H_2O_2 + O_2 \quad (18)$$

$$HO\cdot + HO\cdot \leftrightarrow H_2O_2 \quad (19)$$

$$O_2^-\cdot + O_3 \rightarrow O_3^- + O_2 \quad (20)$$

$$O_3^- + H^+ \rightarrow HO\cdot + O_2 \quad (21)$$

$$NO + O_3 \leftrightarrow NO_2 + O_2 \quad (22)$$

$$2NO_2 + H_2O \rightarrow HNO_2 + HNO_3 \quad (23)$$

$$NO_2 + HO\cdot \rightarrow HNO_3 \quad (24)$$

$$2NO\text{-}2 + 2H^+ \leftrightarrow 2HNO_2 \rightarrow NO\cdot + NO_2\cdot + H_2O \quad (25)$$

$$NO\text{-}2 + H_2O_2 + H^+ \rightarrow ONOOH + H_2O \quad (26)$$

$$ONOOH + H^+ \leftrightarrow HO\cdot + NO_2\cdot \quad (27)$$

Ozone was claimed to play an important role in the degradation of dyes (Garcia *et al.* 2017). However, ozone formation in the air was practically suppressed due to the reaction with nitrogen. In the liquid phase, the O_3 generated O_3^- by exchanging charge with a large number of $O_2^-\cdot$, at a depth of more than 1 μm, which could cause the O_3 concentration to drop rapidly (Olszewski *et al.* 2014). In order to gain further insight into the chemical activity induced by APPJ in the liquid phase, the changes of peroxide, HO·, $O_2^-\cdot$, and RNS were investigated.

Large portions of the short-lived reactive species entered the solution and transformed into long-lived H_2O_2. $ONOO^-$ was also generated in the solution mainly by reaction (24) (Chen *et al.* 2017). As shown in Figure 4(a) and 4(b), the peroxide contents (including H_2O_2 and $ONOO^-$) gradually increased both in the activated water and plasma-treated EBT solution. The peroxide content in the activated water after 6 min treatment was about 1,200 μM, while that in the EBT solution was about 170.00 μM. The peroxide content of the plasma-treated EBT solution was significantly lower than that in the activated water after 3, 4, 5 and 6 min treatments.

The changes of HO· relative content in the activated water and the EBT solution are shown in Figure 4(c). The results clearly show that the HO· content in the plasma-treated solution increased gradually, and was significantly higher than that in the control ($P < 0.05$). Obviously, the relative content of HO· in the EBT solution was dramatically lower than that in the activated water during the whole process ($P < 0.05$). More remarkably, the relative content of HO· in the EBT solution after 0, 1, 2, and 3 min treatment was negative. The negative value indicated that

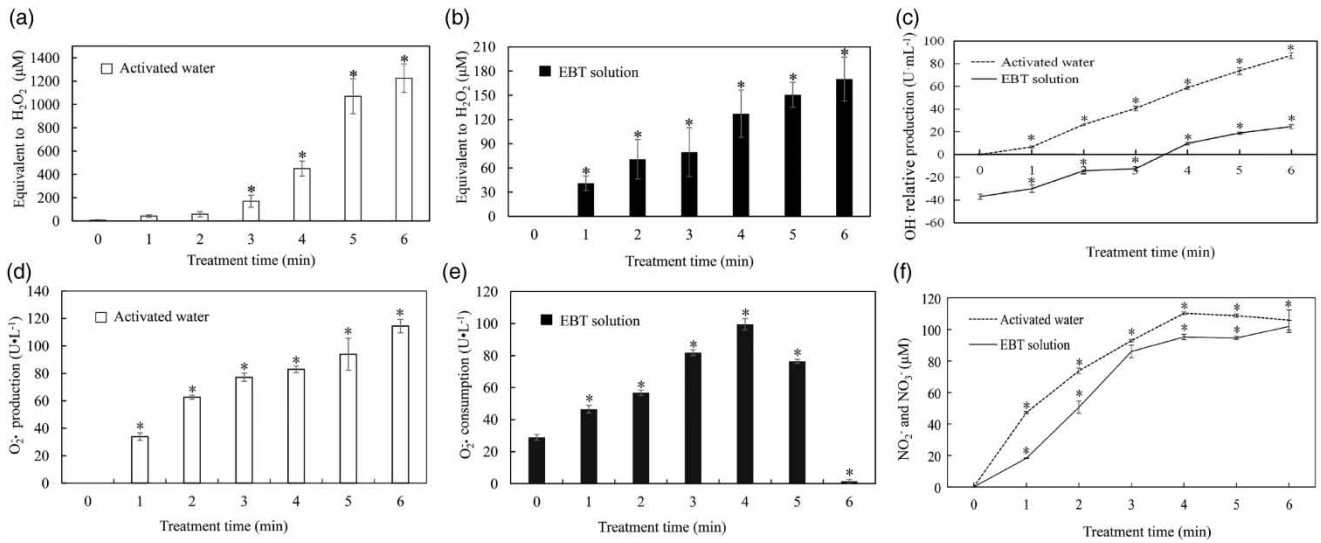

Figure 4 | Changes of RONS in the liquid phase with different treatment times, peroxide (a) (b), HO· (c), $O_2^-\cdot$ (d) (e), NO_3^- and NO_2^- (f). The error bars show the standard deviation of replications. * $P < 0.05$ versus untreated solution.

EBT dye molecules consumed part of the HO· produced in the assay kit, and there was far more HO· consumed by the EBT than there was HO· produced by plasma.

The O_2^-· change in the solution is shown in Figure 4(d) and 4(e). It can be seen that O_2^-· induced by plasma in the activated water gradually increased from 33.89 to 114.47 U·L^{-1}, which was significantly higher than that in the de-ionized water ($P < 0.05$). The EBT dye molecules and the degradation byproducts consumed a large amount of O_2^-·, even exceeding the O_2^-· generated by plasma. The O_2^-· consumption of the EBT solution increased before 4 min plasma treatment and then decreased gradually.

NO· is oxidized to form NO_2^- and later to NO_3^-. The total amount of NO_3^- and NO_2^- was used to represent RNS in the solution. As Figure 4(f) shows, the total NO_3^- and NO_2^- contents gradually increased in plasma-treated solutions, which were significantly higher than those in plasma-untreated liquid ($P < 0.05$). The total NO_3^- and NO_2^- contents of the activated water and EBT solution in 1 and 2 min treatments were 47.10 and 73.68, 18.22 and 50.52 μM, respectively. The total NO_3^- and NO_2^- contents in the activated water were much higher than those in the EBT solution when the plasma treatment time was shorter than 3 min.

Roles of H_2O_2 and HO· on decolorization

CAT is an effective scavenger for H_2O_2 in a solution. The effect of CAT on the decolorization of the EBT solution by APPJ is shown in Figure 5(a). After CAT was added, the decolorization rate of the EBT solution was (9.16 ± 2.01)%, (14.56 ± 0.58)%, (19.95 ± 0.98)%, (38.36 ± 0.30)%, (49.36 ± 1.06)%, and (56.20 ± 0.12)%, respectively, when the plasma exposure was 1, 2, 3, 4, 5 and 6 min. No matter whether there was CAT interference or not, the chromaticity of the treated EBT solution was significantly lower than the original ($P < 0.05$). However, CAT presented an obvious inhibitive effect on the decolorization of the EBT solution, indicating that H_2O_2 played a certain role in the decolorization by plasma.

Figure 5(b) shows the decolorization effect of H_2O_2 alone on the EBT solution. Although the H_2O_2 content in the EBT solution increased largely, A_{525} of the EBT solution decreased slightly. When the H_2O_2 content was 40, 60, 160, 450, 1,050 and 1,200 μM, the decolorization rate was (7.15 ± 0.61)%,

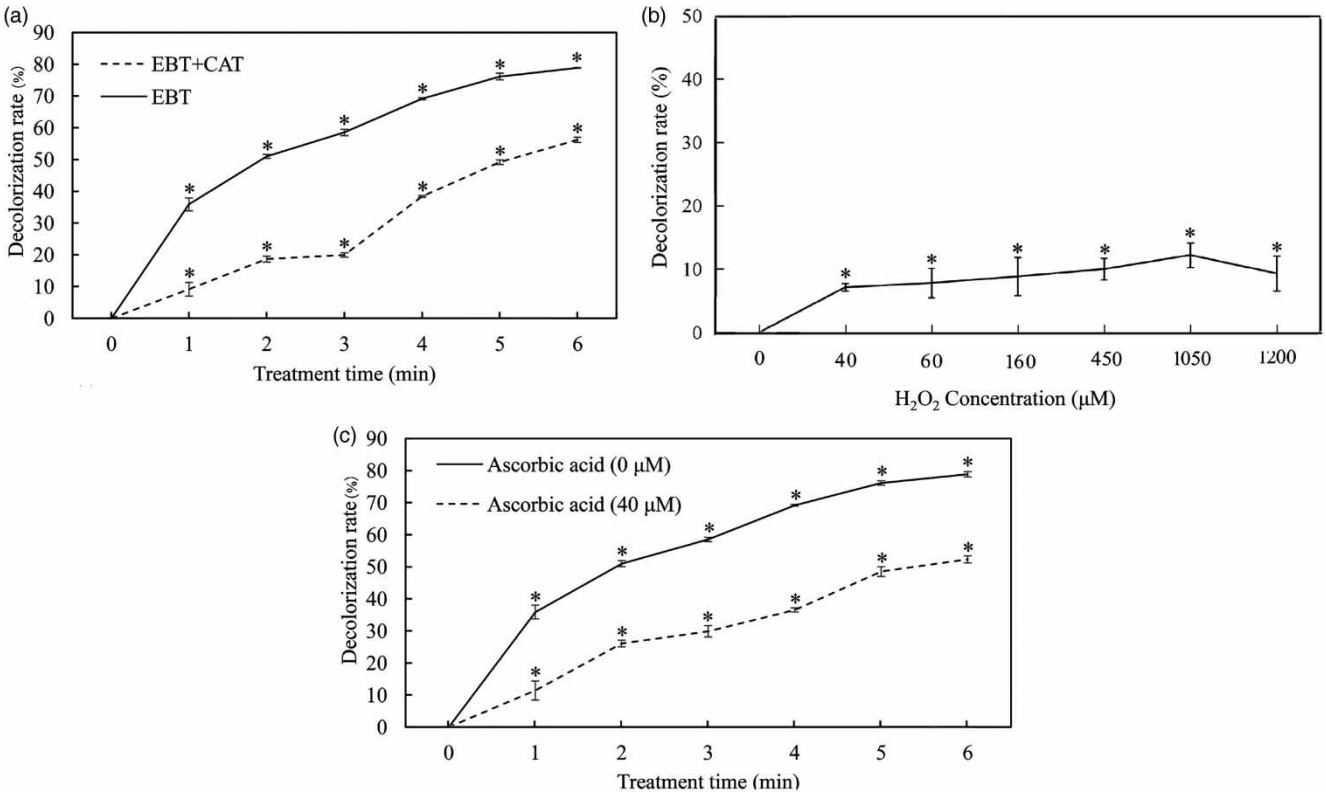

Figure 5 | The effects of CAT (a) and ascorbic acid (c) on decolorization of the EBT solution, the decolorization effect of H_2O_2 alone on EBT solution (b). The error bars showed the standard deviation of replications. * $P < 0.05$ versus untreated solution.

(7.79 ± 2.33)%, (8.83 ± 3.01)%, (10.02 ± 1.71)%, (12.21 ± 1.98)%, and (9.31 ± 2.76)%, respectively, with no significant difference ($P > 0.05$). The decolorization effect of H_2O_2 alone on EBT solution was significantly lower than that of plasma treatment, which indicated that H_2O_2 itself had slight effect on the decolorization of EBT solution.

Ascorbic acid is a typical HO· scavenger. The effect of ascorbic acid on the decolorization of EBT solution by plasma is shown in Figure 5(c). According to a series of pilot experiments, 40 μM ascorbic acid could effectively inhibit the decolorization effect on EBT by plasma. The results showed that, with the addition of ascorbic acid, the decolorization efficiency on EBT solution by plasma decreased obviously.

As HO· is difficult to quantify precisely due to its very short lifetime (Chauvin *et al.* 2017), we chose the method that could reflect the relative trend of HO· in the solution. Obviously, the HO· relative content of plasma-treated EBT solution was much lower than that of the activated water with the same treatment time. HO· is a strong oxidizer that can strongly react with EBT molecules, so the content of HO· in the EBT solution was significantly reduced. Further evidence was that the decolorization effect became obviously weaker with the addition of HO· scavenger. As discussed above, HO· could most likely be the main reactive species responsible for the whole degradation process of dye molecules.

Determination of by-products

The UV/VIS spectra of the EBT solution are shown in Figure 6(a). As could be seen, the EBT solution has a strong absorption peak at 525 nm. This specific absorption peak should be related to the azo bands, the chromogenic groups in EBT, responsible for the visible color of EBT. The absorption in the ultraviolet region is associated with the aromatic structures in EBT molecules. In the first 2 min plasma treatment, the absorbance at 525 nm decreased rapidly; therefore, the azo bond should be the most easily oxidized and broken in the EBT molecules. The intensity of absorption ranging from 280 to 370 nm decreased slightly, indicating that some naphthalene rings were destroyed. When the breakages of –*N*=N– bonds and the aromatic rings occurred, the intensity of absorbance peaks declined gradually in the 280 to 750 nm range.

To further elucidate the related mechanism of the degradation of EBT by plasma, the vibrational spectra of the EBT samples were recorded at several stages during the plasma treatment. Figure 6(b) depicts the FTIR spectra of the EBT solution with plasma exposure of 0, 2, 4, and 6 min. A large number of peaks appeared in the FTIR spectra, which indicated different chemical bonds and the presence of various organic matters.

The broad absorption band at 3,300–3,050 cm^{-1} is related to H-bonded NH symmetric stretching, which appeared in the 2 min EBT sample and disappeared with 6 min treatment. The presence of peaks at 1,651 and 1,538 cm^{-1} is assigned to the deformation of N-H, indicating the breakage of the azo bond and the formation of N-H. The band at ~1,384 cm^{-1} strengthens obviously, which is usually assigned to $-NO_3$ symmetric stretching or O-H deformation or C-O stretching (Wang *et al.* 2016).

The peaks at ~1,605, ~1,562, ~1,504 and ~1,469 cm^{-1} could be assigned to aromatic C = C vibration and the vibration of the benzene ring. The peak at ~3,050 cm^{-1} should be unsaturated C-H stretching vibrations absorption in the benzene ring. The bands at 1,465–1,340 cm^{-1} are assigned to flexural vibration of C-H. The peaks at ~1,208 and 1,048 cm^{-1} are assigned to the stretching vibrations of C-O.

The broad absorption bands at 3,500–3,400 cm^{-1} are attributed to the stretching vibrations of the hydroxyl group and anti-symmetric NH_2 (Tichonovas *et al.* 2013; Bansode *et al.* 2017). The bands in the region at 1,700–1,650 cm^{-1} could be ascribed to C = O stretching vibrations in a carboxylic acid.

The peaks at 1,100 cm^{-1} disappeared after 4 min, the stretching vibrations of the sulfonic acid group. The absorption peaks of the aromatic ring in less than 900 cm^{-1} could be associated with the naphthalene ring, which disappeared after 4 min plasma exposure. The double asymmetric peaks at 2,400–2,300 cm^{-1} are associated with the antisymmetric stretching and deformation vibrations of carbon dioxide.

The azo bonds and aromatic rings were sensitive to the reactive radicals, thus the azo bonds broke and aromatic rings opened in EBT molecules after 4 min plasma treatment. The results of FTIR spectra indicated the degradation by-products of EBT included carboxylic acids, nitrates, amides, and amines.

According to these by-products detected by FTIR analysis and UV/VIS spectra, possible degradation pathways of EBT are proposed (Figure 7). Firstly, the reactive oxygen and nitrogen species attacked the azo bond, leading to the breakage of –*N*=N– and the formation of two different kinds of naphthalene derivatives, which then gradually oxidized to the aromatic compounds with a single aromatic ring. Further oxidation of aromatic rings resulted in the generation of phenolic compounds, ketones, and carboxylic acids, and finally mineralization to CO_2 and H_2O (Shang *et al.* 2017).

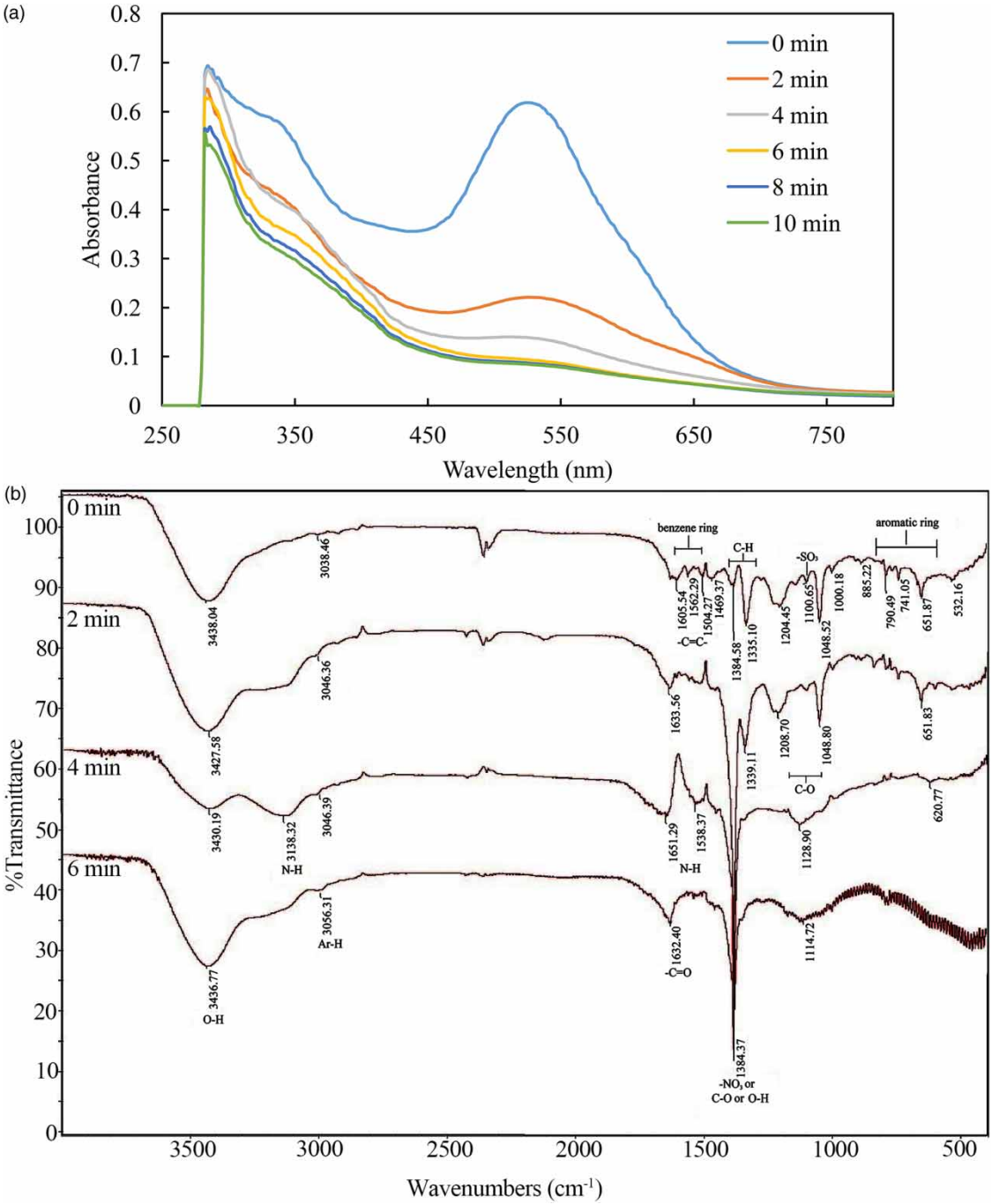

Figure 6 | The residues evolution of EBT solution with different plasma treatment times; (a) UV/VIS spectra, (b) FTIR spectra.

CONCLUSIONS

The results showed that the relatively high decolorization rate (approximately 80%) was obtained after 6 min treatment. The changes and activities of several RONS in the liquid phase were confirmed. The direct oxidation of H_2O_2 to EBT molecules was very weak. During the whole decolorization process, HO· and O_2^-· played crucial roles in the degradation of EBT molecules. However, the oxidation of HO· was nonselective, while the oxidation of O_2^-· was selective, which might effectively destroy the azo bonds and the aromatic rings. The azo chromophoric group was the most

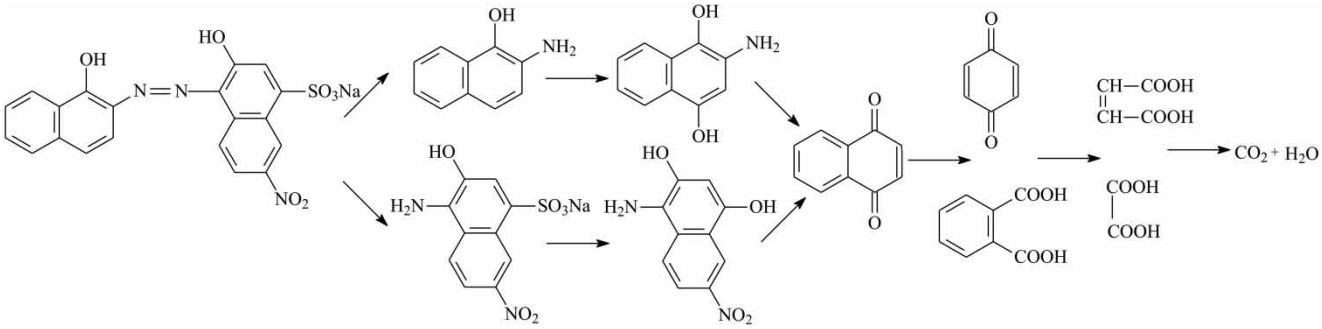

Figure 7 | Possible degradation pathways of EBT by plasma treatment.

easily destroyed in EBT dye molecules. Based on the UV/VIS spectra and FTIR analysis, the azo group and aromatic rings in EBT molecules were destroyed and decomposed into low-molecular by-products. The decolorization experiment proved that APPJ is a very efficient method for the degradation of EBT in water.

ACKNOWLEDGEMENTS

This study was supported by the National Natural Science Foundation of China under Grants 51677146 and the Special Scientific Research Project funds (no. 18JK1102) of Shaanxi Education Department. The authors would like to thank Prof. Ma at the College of Chemistry & Pharmacy, Northwest A&F University, for his excellent technical help.

REFERENCES

Abdelmalek, F., Ghezzar, M. R., Belhadj, M., Addou, A. & Brisset, J.-L. 2006 Bleaching and degradation of textile dyes by nonthermal plasma process at atmospheric pressure. *Industrial & Engineering Chemistry Research* **45**, 23–29.

Bansode, A. S., More, S. E., Siddiqui, E. A., Satpute, S., Ahmad, A., Bhoraskar, S. V. & Mathe, V. L. 2017 Effective degradation of organic water pollutants by atmospheric non-thermal plasma torch and analysis of degradation process. *Chemosphere* **167**, 396–405.

Chauvin, J., Judee, F., Yousfi, M., Vicendo, P. & Merbahi, N. 2017 Analysis of reactive oxygen and nitrogen species generated in three liquid media by low temperature helium plasma jet. *Scientific Reports* **7** (1), 4562.

Chen, C., Li, F., Chen, H.-L. & Kong, M. G. 2017 Aqueous reactive species induced by a PCB surface micro-discharge air plasma device: a quantitative study. *Journal of Physics D: Applied Physics* **50** (44), 445208.

Crini, G. 2006 Non-conventional low-cost adsorbents for dye removal: a review. *Bioresource Technology* **97** (9), 1061–1085.

Djomgoue, P., Woumfo, E. D., Kammoe, A. L., Siewe, J. M. & Njopwouo, D. 2015 Efficiency and chemical recycling capability of magnetite-rich clay towards Eriochrome Black T remediation in the fixed-bed system. *Environmental Technology* **36** (1–4), 281–292.

Garcia, M. C., Mora, M., Esquivel, D., Foster, J. E., Rodero, A., Jimenez-Sanchidrian, C. & Romero-Salguero, F. J. 2017 Microwave atmospheric pressure plasma jets for wastewater treatment: degradation of methylene blue as a model dye. *Chemosphere* **180**, 239–246.

Jiang, B., Zheng, J., Liu, Q. & Wu, M. 2012 Degradation of azo dye using non-thermal plasma advanced oxidation process in a circulatory airtight reactor system. *Chemical Engineering Journal* **204–206**, 32–39.

Kabdasli, I., Ecer, C., Olmez-Hanci, T. & Tunay, O. 2015 A comparative study of HO*- and SO4*–based AOPs for the degradation of non-ionic surfactant brij30. *Water Science and Technology* **72** (2), 194–202.

Kalsoom, U., Bhatti, H. N. & Asgher, M. 2015 Characterization of plant peroxidases and their potential for degradation of dyes: a review. *Applied Biochemistry and Biotechnology* **176** (6), 1529–1550.

Karimi, M. H., Mahdavinia, G. R., Massoumi, B., Baghban, A. & Saraei, M. 2018 Ionically crosslinked magnetic chitosan/kappa-carrageenan bioadsorbents for removal of anionic eriochrome black-T. *International Journal of Biological Macromolecules* **113**, 361–375.

Karthikeyan, S., Boopathy, R. & Sekaran, G. 2015 In situ generation of hydroxyl radical by cobalt oxide supported porous carbon enhance removal of refractory organics in tannery dyeing wastewater. *Journal of Colloid and Interface Science* **448**, 163–174.

Krugly, E., Martuzevicius, D., Tichonovas, M., Jankunaite, D., Rumskaite, I., Jolanta Sedlina, V. R. & Baltrusaitis, J. 2015 Decomposition of 2-naphthol in water using a non-thermal plasma reactor. *Chemical Engineering Journal* **260**, 188–198.

Liu, J. R., Xu, G. M., Shi, X. M. & Zhang, G. J. 2017 Low temperature plasma promoting fibroblast proliferation by activating the NF-kappaB pathway and increasing cyclind1 expression. *Scientific Reports* **7** (1), 11698.

Olszewski, P., Li, J. F., Liu, D. X. & Walsh, J. L. 2014 Optimizing the electrical excitation of an atmospheric pressure plasma

advanced oxidation process. *Journal of Hazardous Materials* **279**, 60–66.

Rawat, D., Sharma, R. S., Karmakar, S., Arora, L. S. & Mishra, V. 2018 Ecotoxic potential of a presumably non-toxic azo dye. *Ecotoxicology and Environmental Safety* **148**, 528–537.

Setsuhara, Y. 2016 Low-temperature atmospheric-pressure plasma sources for plasma medicine. *Archives of Biochemistry and Biophysics* **605**, 3–10.

Shang, K., Wang, X., Li, J., Wang, H., Lu, N., Jiang, N. & Wu, Y. 2017 Synergetic degradation of Acid Orange 7 (AO7) dye by DBD plasma and persulfate. *Chemical Engineering Journal* **311**, 378–384.

Shi, X.-M., Liao, W.-L., Chang, Z.-S., Zhang, G.-J., Wu, X.-L., Dong, X.-F., Yao, C.-W., Ye, B.-Y., Li, P., Xu, G.-M., Chen, S.-L. & Cai, J.-F. 2015 Inactivation effect of low-temperature plasma on pseudomonas aeruginosa for nosocomial anti-infection. *IEEE Transactions on Plasma Science* **43**, 3211–3218.

Shi, X., Liu, J., Xu, G., Wu, Y., Gao, L., Li, X., Yang, Y. & Zhang, G. 2018 Effect of low-temperature plasma on the degradation of omethoate residue and quality of apple and spinach. *Plasma Science and Technology* **20** (4), 044004.

Tichonovas, M., Krugly, E., Racys, V., Hippler, R., Kauneliene, V., Stasiulaitiene, I. & Martuzevicius, D. 2013 Degradation of various textile dyes as wastewater pollutants under dielectric barrier discharge plasma treatment. *Chemical Engineering Journal* **229**, 9–19.

Tran, V. S., Ngo, H. H., Guo, W., Ton-That, C., Li, J., Li, J. & Liu, Y. 2017 Removal of antibiotics (sulfamethazine, tetracycline and chloramphenicol) from aqueous solution by raw and nitrogen plasma modified steel shavings. *Science of the Total Environment* **601–602**, 845–856.

Vilar, V. J. P., Amorim, C. C., Brillas, E., Puma, G. L., Malato, S. & Dionysiou, D. D. 2017 AOPs: recent advances to overcome barriers in the treatment of water, wastewater and air. *Environmental Science and Pollution Research International* **24** (7), 5987–5990.

Wang, T., Qu, G., Ren, J., Yan, Q., Sun, Q., Liang, D. & Hu, S. 2016 Evaluation of the potentials of humic acid removal in water by gas phase surface discharge plasma. *Water Research* **89**, 28–38.

Zaghbani, N., Hafiane, A. & Dhahbi, M. 2009 Removal of Eriochrome Blue Black R from wastewater using micellar-enhanced ultrafiltration. *Journal of Hazardous Materials* **168** (2–3), 1417–1421.

First received 23 August 2018; accepted in revised form 21 March 2019. Available online 5 April 2019